Aptamer biosensing based on metal enhanced fluorescence platform: a promising diagnostic tool

Savita M. Sundaresan[1], S M Fothergill[1], Tanveer A. Tabish[1], Mary Ryan[1], Fang Xie[1,*]

[1] Department of Materials and London Centre for Nanotechnology, Imperial College London, London, SW7 2AZ, United Kingdom.

[*] **Corresponding author: Fang Xie (email: f.xie@imperial.ac.uk)**

Abstract

Diagnosis of disease at an early, curable and reversible stage allows more conservative treatment and better patient outcomes. Fluorescence biosensing is a widely used method to detect biomarkers, which are early indicators of disease. Importantly, biosensing requires a high level of sensitivity. Traditionally, these sensors use antibodies or enzymes as biorecognition molecules, however these can lack the specificity required in a clinical setting, limiting their overall applicability. Aptamers are short, single stranded nucleotides that are receiving increasing attention over traditional recognition molecules. These exhibit many advantages, such as high specificity, making them promising for ultrasensitive biosensors. Metal enhanced fluorescence (MEF), utilises plasmonic materials, which can increase the sensitivity of label-based fluorescent biosensors. The fluorescence enhancement achieved by placing metallic nanostructures in close proximity to fluorophores allows for detection of ultra-low biomarker concentrations. Plasmonic biosensors have been successfully implemented as diagnostic tools for a number of diseases, such as cancer, yet reproducible systems exhibiting high specificity and the ability to multiplex remain challenging. Similarly, whilst aptasensors have been extensively reported, few systems currently incorporate MEF, which could drastically improve biosensor sensitivity. Here, we review the latest advancements in the field of aptamer biosensing based on MEF that have been explored for the detection of a wide variety of biological molecules. While this emerging biosensing technology is still in its infant stage, we highlight the potential challenges and its clinical potential in early diagnosis of diseases.

1. Introduction

Early disease diagnosis is crucial in order for patients to access earlier treatment and maximise survival rates.[1] Patients often do not present visible symptoms at the onset of some diseases (for example, certain cancers such as pancreatic and prostate) hence, they go undiagnosed until very advanced stages, at which point treatment is less effective and survival rates are lower.[1-5] This means that early detection is the only viable method of preventing some diseases from progressing. Biosensing is a simple and sensitive technique that can be used to detect low abundance disease biomarkers in the body.[6] Biosensors are devices designed to detect the presence of specific analytes in the body (usually proteins, peptides, antigens or other small molecules) and convert it into a detectable and easy processible signal that can

be quantified. In general terms, a biosensor consists of a biorecognition molecule, to specifically detect the biomarker and a transducer, to convert this into a signal that is proportional to the concentration of an analyte.[6] Patient samples such as blood, urine or saliva are the most widely used, as biomarkers are usually found in high concentrations in these fluids. Biosensing was introduced in the 1960s and since then it has been successfully implemented for the detection of various biomarkers such as glucose and human interleukin.[7] The enzyme-linked immunosorbent assay (ELISA) is a widely used method for biosensing, capable of measuring very low concentrations of molecules with high specificity against the antibodies or antigens developed for them.[8] Various types of biosensors have been investigated such as optical, electrochemical, magnetic and piezoelectric. Optical biosensing is one of the most commonly reported class of sensing and can be either label-free or label-based. In a label-free mode, the signal is produced due to direct interaction between the analyte and transducer, whereas label-based sensors involve the use of a label which in turn generates an optical signal. These can be measured via their fluorescence, absorbance, reflectance, scattering or luminescence.[6] Optical biosensors utilise various biological materials as biorecognition molecules including antibodies and antigens, and is frequently used in the optical ELISA assay, however can also use enzymes and aptamers.[6] Fluorescence biosensing in particular is a commonly used method, employing fluorophores in the ultra-violet (UV), visible, to infrared (IR) range to convert biomarker detection into a fluorescence signal that can be measured and quantified in correspondence to analyte concentration. For clinical use, biosensors must be reproducible, cost effective and must demonstrate fast detection times. Though optical sensors have been routinely used in readout assays for many years, plasmonic materials have been shown to considerably improve the signal to noise ratio by amplifying the fluorescence intensity through metal enhanced fluorescence (MEF).[9-10] This review, for the first time, focusses on the recent work incorporating aptamer biosensing based on MEF for highly sensitive biomarker detection. Moreover, we explore how plasmonic materials, incorporated into aptamer sensing systems are advantageous for developing multiplexing systems, whereby a panel of multiple biomarkers can be quantified simultaneously.

Aptamers are short, single strands of DNA or RNA that can specifically bind to a wide range of target molecules, including proteins.[11-12] Discovered in the early 1990s, aptamers are often referred to as 'chemical antibodies' due to their artificial production by the systematic evolution of the ligand by the exponential enrichment process (SELEX).[13] Briefly, this process involves incubation of a random library of nucleic acids with a target biomarker, where the repeated separation of bound and unbound nucleic acids results in a final enriched library of highly specific aptamers. Although aptamers have been studied for the development of drugs and drug delivery systems but are primarily been investigated as diagnostic and therapeutic tools.[14] Since their discovery in 1990, aptamers have been found to bind to a wide range of target molecules such as proteins, amino acids and even whole cells. Recently, in-depth understanding of various aptamer morphologies and conformations have allowed for complex biosensing mechanisms with high specificity.[15]

Though antibodies are the most well-studied and highly used biorecognition molecules, there are many cases where antibodies may not be available as it may not be possible to produce an antibody against a specific antigen or one that has a particular chemical modification.

PLEASE CITE THIS ARTICLE AS DOI: 10.1063/5.0065833

Additionally, antibodies may not possess the required specificity and are known to suffer batch-to-batch variation and short shelf-life.[16] Discovered nearly 30 years ago, nanobodies have also been investigated as an alternative novel class of antigen-binding fragments derived from the Alpaca heavy chain IgG antibody, displaying superior properties such as high stability, small size, strong antigen-binding affinity and reversible unfolding.[17]

Enzyme based biosensors are another very commonly utilised class, conventionally used in optical and electrochemical sensors.[18-19] In a successful enzyme based biosensor, the enzyme must be stable under normal conditions and must be able to catalyse a specific biochemical reaction in the presence of a target biomarker.[19] There are several benefits of using enzymes including high specificity, catalytic activity and their ability to work at raised potentials, allowing for electrochemical transduction.[20] Enzyme based biosensors are most commonly designed to detect glucose, lactate and cholesterol, with many having already been commercialised for the self-monitoring of blood glucose levels.[19] However, enzymes are limited in that they can only operate within a certain temperature range to avoid thermal denaturation.[20]

More recently, 'bottom-up' methods such as DNA origami have enabled construction of complex nanostructures with high potential in biosensing. DNA origami involves self-folding of long single-stranded DNA, using hundreds of short, complementary oligonucleotides and has the ability to form two and three dimensional structures, such as sheets or more complex structures with edges and planes.[21] These DNA structures can be tuned to respond to external stimuli, such as biological molecules, enabling their use for biosensing applications.[22] DNA origami binds to target molecules in a similar way to aptamers in that they are able to undergo conformational changes upon detection of a specific molecule. These dynamic structural changes can then be detected through optical or electrochemical means.[23] The types of conformational changes that aptamers undergo upon target detection will be expanded on in Section 4. DNA origami also display many advantages over antibodies, primarily, their small size, high stability and dynamic structure, which can undergo large conformational changes.[23] However, as these structures are so complex, maintaining their structural integrity in different media may pose as a limitation.[24] DNA origami is usually produced in buffers supplemented with Mg^{2+} and has been found to denature in Mg^{2+}-free buffers. Since these required buffer conditions may not always be compatible with the system under investigation, for instance they may interfere with fluorescence activity, it poses a limitation of the use of these structures in biosensing applications.[25] Fig. 1 shows the structure and size comparison of these biorecognition molecules.

Aptamers have exhibited unprecedented advantages over other biorecognition markers, making them ideal recognition elements in biosensing (shown in Table I).[15] Aptamers are small in size, possess high specificity, ease of modification, long shelf-life, reversible denaturing and high cost effectiveness when compared to antibodies.[12, 15, 26] They have also exhibited lower limits of detection (LODs) and faster response times when compared to antibodies, making them ideal for biosensing.[15, 27] For example, when the response times for insulin detection were directly compared between aptamers and antibodies under biologically relevant and identical conditions, they exhibited a response times of 12 minutes and 60 minutes respectively. In this study, a faster response time of the aptamers was attributed to their unique conformational change during the interaction with insulin, allowing

rapid binding. The aptamer modified surfaces also presented a lower detection limit, highlighting their superior sensing performace.[27] Additionally, unlike other biorecognition molecules, aptamers can function in alkaline or acidic conditions, allowing for the possibility of targeting biomarkers in complex media and non-physiological conditions.[28] Although aptamers possess similar, if not superior binding affinity for their targets to antibodies,[29] their ability to undergo significant conformational changes upon target binding, offers great flexibility in the design of novel biosensors with high selectivity and sensitivity.[15] This is specifically advantageous for multiplexed systems. Moreover, due to their small size, they can be arranged with a high surface density on biosensor surfaces, allowing for higher concentration detection of biomarkers.

Table I: Pros and cons of using antibodies, nanobodies, DNA origami and aptamers in biosensing.[24, 28]

Conditions	Antibodies	Nanobodies	DNA origami	Aptamers
Use in physiological conditions (e.g. pH, temp)	✓	✓	✓	✓
Use in non-physiological conditions	×	×	×	✓
Complex target selection	✓	✓	✓	✓
Stability in wide temperature range	×	×	×	✓
Immunogenicity	✓	✓	✓	Limited

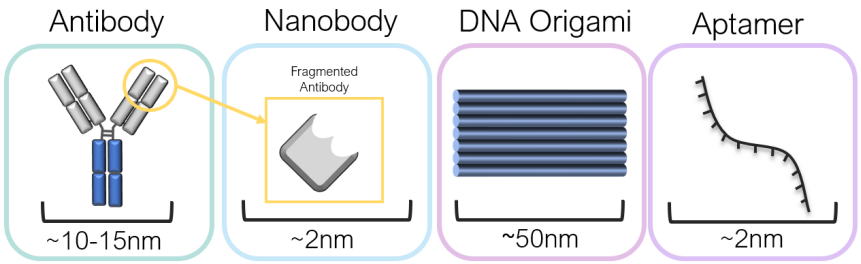

Figure 1: Schematic structures of biorecognition molecules

Despite numerous advantages, there is limited literature on MEF based aptamer sensors. This could be because the incorporation of aptamers in biosensing technology is relatively new in comparison to antibodies, which are well-established as biorecognition molecules. The aptamer generation process is also more tedious than acquiring antibodies, which are widely available against multiple disease biomarkers. Although the process of making known aptamer sequences is relatively cost-efficient compared to antibodies, generating a new aptamer against a particular biomarker can be a long process. However, methods such as automated SELEX and capillary electrophoresis SELEX can enable aptamers with the required characteristics and binding parameters to be generated in several days.[30] Additionally, aptamers that are generated in the same conditions against the same target may differ in structure, specificity and other properties. However, falling costs of chemical synthesis and increasing aptamer databases have great potential to facilitate mass of production of aptamers with high reproducibility and reliability.[30]

This review summarises the latest advancements in the field of aptamer biosensing based on MEF platform. The rational design of plasmonic nanostructures are explored for the detection of a wide variety of biological molecules, with both solution- and substrate-based sensing formats. Lastly, while this emerging biosensing technology is still in its infant stage, the potential challenges and clinical potential of this emerging biosensing technology are highlighted.

2. Metal enhanced fluorescence (MEF)

Metal enhanced fluorescence (MEF) is a phenomenon that fluorescence signal is amplified when a fluorophore is in close proximity of metal nanoparticles. Although the theory behind this phenomenon had been developed since the 1980s, its application in biosensing is relatively new.[31] MEF occurs when light is incident on a conducting metallic nanoparticle (NP) and couples with the layer of free electrons oscillating at a fixed frequency on the NP surface. At a particular frequency of light, localised surface plasmon resonance (LSPR) occurs, leading to the collective but non-propagating oscillations of surface electrons, which can generate a localised enhanced electric field near the NP (Fig. 2b). As a result, any proximal fluorophores will couple with the metallic NP and experience a light intensity several orders of magnitude higher than the actual incident intensity, so that the energy of free propagation is converted into localised near field energy (Fig. 2c). This results in many desirable characteristics such as increased fluorophore intensity, increased quantum yield and decreased lifetime, leading to higher photostability as the fluorophores spend less time in an excited state.[32]

Although the actual mechanism of MEF is still debated, three main mechanism pathways proposed in 2002 by Geddes *et al.* are widely accepted.[32] Of these three mechanisms, two are related to the enhancement of the fluorophore and one is related to its quenching. The first enhancement mechanism proposed is attributed to the increased local electric field around the metal nanoparticle surface, increasing the rate of excitation of the nearby fluorophore. The second, is that any nearby metal nanoparticle can increase the radiative decay rate of the fluorophore (i.e. the rate at which a fluorophore emits photons). The third mechanism is the energy transfer quenching of the fluorophore which occurs due to damping of the dipole oscillations by the metal.[31] The simplified Jablonski diagram is a commonly used

way of visualising the enhancement mechanisms (Fig. 2c).[32] Absorption of incident light sends the fluorophore into an excited state, after which the excited electrons undergo internal conversion and relax to the lowest vibrational energy before emitting a photon of a longer wavelength and returning back to the ground state. This could happen via a radiative, non-radiative or quenching decay route.[32]

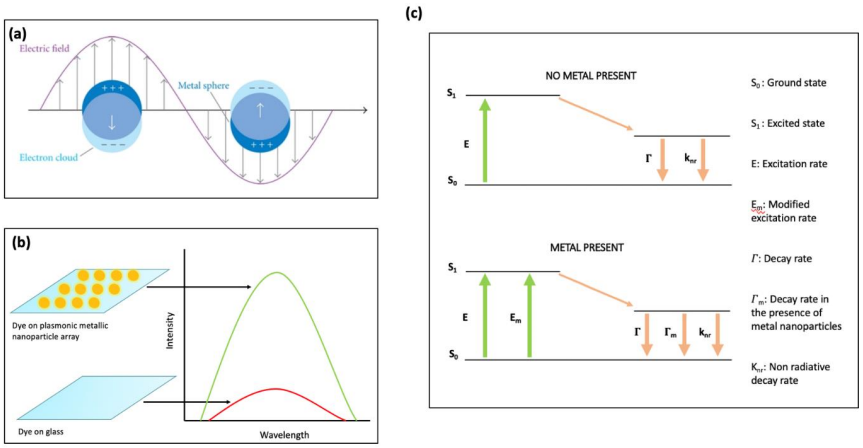

Figure 2: (a) Mechanism of localised surfaced plasmon resonance.[33] Reproduced with permission from Joyce *et al.*, Elsevier (2020). Copyright 2020 Elsevier. (b) Difference in fluorescence intensity between glass substrate and plasmonic substrate (c) Simplified Jablonski diagram showing increases in excitation and radiative decay rates in free space and in presence of metallic nanoparticles.

The emission of isolated and coupled fluorophores can be modelled mathematically using formulae in terms of their quantum yield (Q_0) and their lifetime (τ_0) where the subscript '0' indicates the fluorophore is not in the presence of a metal NP. Q_0 reflects the proportion of radiative to non-radiative decay of a fluorophore.[32] This is generally thought to increase via a reduction in the non-radiative (k_{nr}) and quenching (k_q) decay rates.

$$Q_0 = \frac{\Gamma}{\Gamma + k_{nr} + k_q} \quad (1)$$

$$\tau_0 = \frac{1}{\Gamma + k_{nr} + k_q} \quad (2)$$

When placed near the metallic NPs, fluorophores can undergo modifications to their radiative decay rates Γ_m, which generally increases their quantum yield and reduces their lifetime.

$$Q_m = \frac{\Gamma + \Gamma_m}{\Gamma + \Gamma_m + k_{nr} + k_q} \quad (3)$$

$$\tau_m = \frac{1}{\Gamma + \Gamma_m + k_{nr} + k_q} \quad (4)$$

Since the overall plasmonic enhancement is given by the product of the modified quantum yield and the enhanced excitation rate, it can be expressed as the following.[9]

$$\Gamma_{fl} = Q_m \cdot \Gamma_{ex} = \frac{\Gamma + \Gamma_m}{\Gamma + \Gamma_m + k_{nr} + k_q} \cdot \Gamma_{ex} \quad (5)$$

When the fluorophore and metal NP are at large separations, the modified decay rate (Γ_m) decreases and new decay channels cannot be created as the NP is too far away to have an effect, hence the unmodified quantum yield is attained. Contrastingly, at very small separation distances (below 5 nm), quenching of the fluorophore occurs so Q_m goes to 0.

3. Plasmonic nanostructures for biosensing

As MEF has the capability of increasing the fluorophore intensity, it can be utilised in fluorescent biosensing to produce detectable fluorescent signals from very low biomarker concentrations, resulting in highly sensitive biosensors. The architecture of the NP (i.e. the size, morphology, dielectric constant and particle separation distance) determines the electric field enhancement and LSPR of the NP and can be tuned for maximum fluorophore enhancement.[34] Most importantly, the NP LSPR has to overlap with the optical properties of the fluorophore to enable simultaneous excitation using the excitation source. MEF has been used in solution and substrate based sensing, using fluorophores with a wide range of excitation and emission wavelengths from the UV to near infrared (NIR) II regions.[9] Biosensing typically takes place in this wavelength region as the most commonly used plasmonic materials such as gold and silver have plasmonic absorption peaks in this range. In recent years, there has been a shift towards biosensing and imaging in the NIR I and II regions, particularly between 650 - 950 nm.[9] The presence of haemoglobin and larger proteins in patient samples can reduce the fluorescence intensity as they absorb shorter wavelengths of light, hence longer excitation and emission wavelengths are desirable. However, to date, the large majority of plasmonic aptasensors function in the visible region hence, shifting aptamer-based sensing into the NIR I and II regions has potential to propel the field of biosensing. In the past decade, MEF has been devised and implemented extensively in biosensing and has shown to improve detection limits of different biomarkers. For example, pancreatic cancer biomarker CA 19-9 has been shown to have a detection limit of 0.6 U/mL using standard ELISA kits, however incorporation of MEF into a CA 19-9 immunoassay has improved this by several orders of magnitude to 7.7 x 10^{-7} U/mL.[35-36] Although the majority of MEF biosensors have implemented antibodies, aptamers are receiving increased attention in these systems for their versatile configurations and high specificity.

Nanostructure morphology plays a crucial role in fluorophore enhancement and ultimately determines the overall sensitivity of the biosensor. Over the past two decades, huge progress has been made in the synthesis of monodisperse, reproducible nanostructures, particularly that of gold and silver. Yaraki *et al.* have extensively reviewed numerous plasmonic morphologies for biosensors, concluding that anisotropic particles in particular possess high enhanced electric fields and extinction wavelengths over a broad range from the visible to IR region.[37] Gold and silver nanostructures are the most frequently used as plasmonic materials due to their strong plasmonic features, high stability, biocompatibility and ease of functionalisation.[33, 38-40] Other plasmonic materials include palladium[41], copper[42], iron

disulfide[43] and semiconductors such as titanium nitride[44] and copper sulfide[45]. The morphology of the NP also plays an important role in the enhancement. Whilst nanospheres,[39] nanodiscs,[46] nanorods,[47] and nanotriangles[48] are all established morphologies, many MEF aptasensors have recently implemented more complex, anisotropic structures such as nanobipyramids,[49] dendrites,[50] and core-shell particles[51].

Simple morphologies such as gold nanospheres are easier to fabricate, however their plasmon wavelength can only be tuned over a small range of wavelengths, from 520 nm to 640 nm[52], limiting their applicability for sensing. Gold nanobipyramids have gained enormous attention over the last decade as plasmonic structures, offering a much higher electromagnetic enhancement than nanorods, due to the lightening rod effect as a result of their sharp tips. By tailoring their aspect ratio, the plasmon resonance can be tuned over a wide range spectral range covering the NIR I and II regions.[52] Bipyramids offer many other advantages such as high chemical stability, large optical cross sections and a higher refractive index than rods.[52] Recently, Zhu *et al.* demonstrated the tunability of these structures by capping gold bipyramids with AgPd, resulting in a broadening of the LSPR and red shift of ~900 nm (Fig. 3a). They were also shown to produce a high photothermal conversion efficiency and good photothermal therapy performance.[53] Nanocubes are another promising plasmonic structure, displaying strong LSPR peaks originating from their sharp corners. Gold nanocubes in particular have been shown to produce electric field enhancement factors more than 17 times higher than gold spheres (Fig. 3b).[54] Other materials such as silver[55]and iron sulfide[43] have been used for cubic structures. These structures have been successfully implemented in biosensing, for example, in 2014, Xu *et al.* obtained an enhancement factor of 2 orders of magnitude using gold nanocubes for the detection of aluminium phthalocyanines in cancer cells.[56] Furthermore, in 2017, core-shell nanocubes grafted with rhodamine were implemented for the detection of mercury ions for MEF and SERS.[57] Hollow metallic nanostructures have been utilised in biosensing, drug delivery and catalysis in recent years, outperforming their solid counterparts. Controlled synthesis of uniform shells can result in enhanced plasmonic properties, due to the effective dipole mode of a dielectric void and shell which generates plasmon hybridisation. This results in splitting and shifting of plasmon resonances and enhances the local electromagnetic field.[58] Although these complex structures have the potential to produce high enhancements, they must meet several requirements in order to be utilised in an aptasensor system for clinical use, particularly high reproducibility and long-term stability. This poses as a challenge for more complex structures as the addition of layers, spikes and other shapes limits uniformity.

For substrate based sensing, several lithographic techniques have been employed for uniform, large-scale nanoarrays.[33] Nanohole-disc arrays, for example, can be produced via low-cost lithographic techniques and have been shown to display enhancements of over 400 times due to the combination of LSPR and surface plasmon polariton (SPP), as demonstrated by Pang *et al.* in 2019 (Fig. 3c).[59] In contrast to LSPR, SPPs are propagating electromagnetic waves that travel across the interface of metal-dielectric films with wavelengths in the NIR and visible regions. These cannot be excited by free space radiation, instead they require matching momentum such as periodicity in order for resonance excitation. The enhancement of the electromagnetic field at the interface results in fluorescence enhancement.

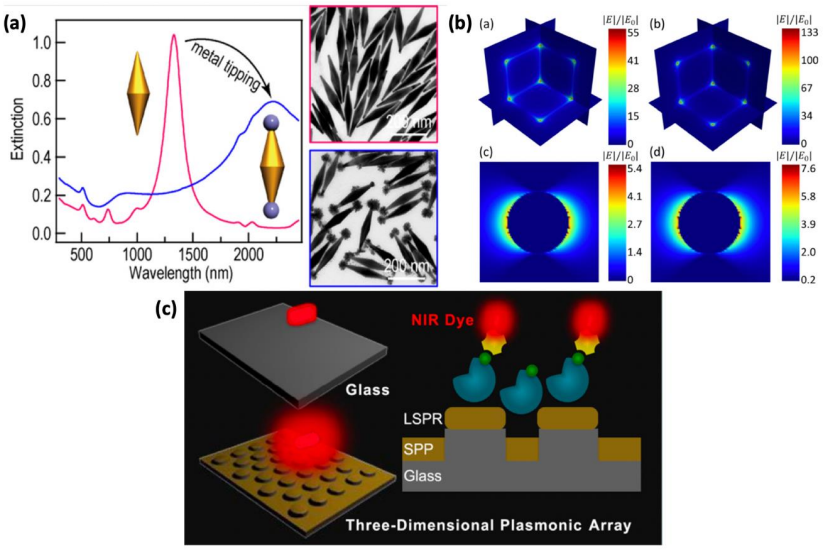

Figure 3: a) Extinction spectra and TEM images of AgPd capped gold nanobipyramids.[53] Reproduced with permission from Zhu *et al.*, Journal of the American Chemical Society 139 (39), 13837-13846 (2017). Copyright 2017 Journal of the American Chemical Society. b) Comparison of the modelled electric field enhancement of gold and copper cubes a) Copper cube b) Gold cube c) Copper sphere d) Gold sphere.[54] Reproduced with permission from Zheng *et al.,* from Nano Research 12 (1), 63-68 (2019). Copyright 2019 Nano Research. c) Schematic of gold nanohole-disc arrays showing generation of SPP and LSPR.[59] Reproduced with permission from Pang *et al., ACS* Applied Materials & Interfaces 11 (26), 23083-23092 (2019). Copyright 2019 ACS Applied Materials & Interfaces. Further permissions related to the material excerpted should be directed to the ACS.

4. MEF aptamer-based sensors

Unlike antibody detection systems, which are much more rigid, aptamers can be cleaved and can undergo conformational changes. This permits quenching to enhancement mechanisms, whereby the background noise of the system can be reduced to zero during non-specific binding, providing a much clearer signal. Generally, fluorescent plasmonic aptamer systems can be designed as either "turn on" or "turn off" sensors (Fig. 4). In "turn on" systems, a fluorophore and nanoparticle are initially held in close proximity to each other by an aptamer, resulting in quenching of the fluorophore. After specific target binding of the aptamer to the biomarker, the aptamer will detach from the nanoparticle or undergo a conformational change, resulting in a recovery of the fluorescence. In "turn off" systems, the reverse occurs, whereby selective binding of the target and aptamer drives the fluorophore closer to the NP and results in quenching.

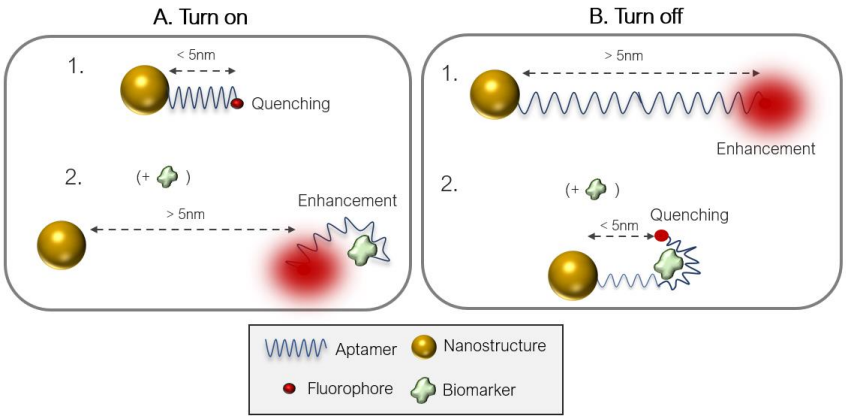

Figure 4: Illustration of "Turn on" and "Turn off" aptamer systems. In a "turn on" system, the fluorophore is initially quenched by the nanoparticle and upon biomarker detection, the aptamer breaks away enabling amplification of fluorophore intensity. In "turn off" systems, the reverse occurs.

Aptamer-based bioassay interactions can be further categorised by the different configurations and conformational changes they undergo upon biomarker detection (Fig. 5). Simple binding assays are frequently used, where aptamers can directly replace antibodies. Targeted binding to immobilised aptamers can produce an optical signal which can be measured through various mechanisms such as ELISA, mass or refractive index change (Fig. 5a). Sandwich assays in particular show higher specificity than direct binding assays, utilising two complimentary aptamers to detect the target biomarker. In this method, capture aptamer probes can be immobilised onto a surface (e.g. a glass substrate or a nanoparticle) and a report aptamer can be signalled with a fluorescent tag such as a fluorophore or quantum dot. FRET based detection is a widely used aptamer detection mechanism, based on the quenching of fluorophores due to target induced aptamer conformational changes.[12] FRET traditionally involves non-radiative energy transfer between a donor fluorophore and acceptor fluorophore whereby graphene oxide is commonly employed as an efficient FRET fluorophore quencher (Fig. 5b).[60]

While antibody target binding does not involve conformation changes, aptamers are known for target induced structure switching. In these sensors, aptamers are designed to switch between two distinct structures, where one configuration leads to a signal increase (Fig. 5c).[61] These configurations are varied and range from target induced aptamer aggregation to split aptamer assembly, allowing for signal enhancement or recovery (Fig. 5d-f). G-quadruplex secondary structures in particular constitute a unique class of nucleic acid structures, widely utilised in structure switching mechanisms and depending on their loop lengths and sequences, can exhibit high stability and highly specific target detection.[62] Hybridisation reactions are another example of a structure switching chain reaction. In simple terms, a hybridisation reaction is where a single-stranded DNA initiator opens up a hairpin DNA of one

species, exposing a new single stranded region which in turn, exposes another single stranded region of another species, resulting in the formation of a double helix that can be detected by conjugation of fluorophores.[63] In addition, target induced displacement is a frequently used mechanism for detection where target-aptamer complexes are displaced into solution and produce a detectable change in signal. This could take place via a strand displacement reaction, where an invader DNA/RNA biomarker strand can attach to toe-holds (single stranded segments of DNA) and result in displacement of aptamers into solution. This mechanism has been utilised for the detection of miRNA by Zhu *et al.*[61, 64] Although many aptamer sensing mechanisms are available, the type of binding mechanism occurring in any system heavily relies on the aptamer structure and the type of biomarker being detected.

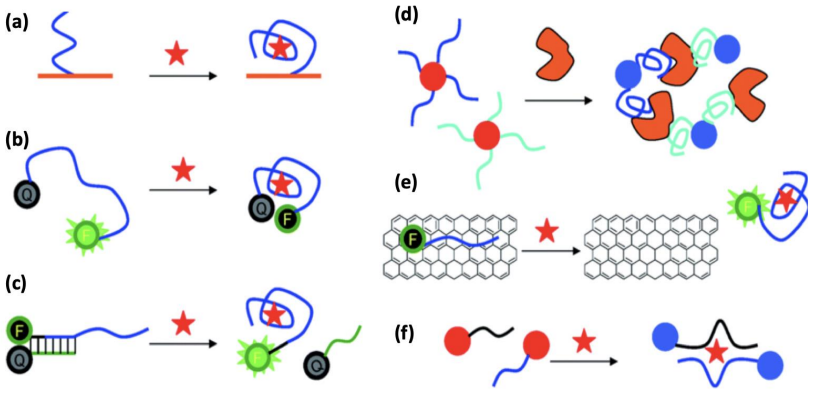

Figure 5: Aptamer configurations in various biosensor systems (a) Simple binding assay whereby the target biomarker can be detected through ELISA, mass or refractive index change. (b) Fluorescence resonance energy transfer (FRET) based sensor based on target induced aptamer conformation change. (c) Structure switching system where target binding results in signal recovery of the fluorophore (d) Detection based on target induced nanoparticle aggregation mechanism (e) Graphene oxide based system where target binding results in fluorescence recovery (f) Detection of target biomarker results in split aptamer binding resulting in nanoparticle assembly.[61] Reproduced with permission from Zhou *et al.*, Analyst 139 (11), 2627-2640 (2014). Copyright 2014 RSC Publications.

There are many design considerations when selecting an aptamer for a plasmonic sensing system. Firstly, the length of the aptamer should be between 5 – 90 nm to maintain optimal distance between the metallic nanostructure and fluorophore.[65] The aptamer should also have a stronger affinity for its biomarker than the NP and should specifically bind to its biomarker to avoid false positive signals. Lastly, the aptamer should be able to bind to the dye and NP on either side without affecting the plasmonic properties of the system.[12] The majority of these MEF aptasensor systems are solution based, in comparison to antibody biosensing, which is largely substrate based, allowing for *in vivo* imaging.[9, 33] This may be due

to the fact that "on-off" mechanisms are more compatible with nanoparticles in solution, where aptamers have a larger surface area on the NP to undergo conformational changes. These "on/off" systems have been widely reported for a variety of different biomarkers and fluorophores.[66-70] In 2017, Jin *et al.* reported a NIR "turn on" probe for the detection of ovarian cancer biomarker CA 125.[69] Here, Ag_2S quantum dots were used to quench an aptamer/5-fluorouracil complex through photo-induced electron transfer. Biomarker detection resulted in specific binding to the aptamer/5-fluorouracil complex, separating it from the quantum dot, inducing NIR photoluminescence recovery.[69]

Solution based aptasensing can be carried out in a similar way to substrate based sensing, whereby patient samples can be directly added into a nanoparticle solution and read using a photoluminescence machine or a well plate reader. However, in practice, solution based sensing is more challenging as unconjugated dye and biomarkers must be centrifuged out rather than being washed out, limiting the viability of ELISA based assays. The following sections review recent developments in solution- and substrate-based MEF aptasensors.

5.1 Solution based MEF aptasensors

As early as 2012, detection limits of 200 nM have been obtained using silver NPs in an aptamer based adenosine detector by Wang *et al.*[71] Later, in 2013, Choi *et al*. reported AuNPs for the quenching and fluorescence of fluorescein isothiocyanate (FITC) dye in the visible range, for prostate specific antigen (PSA) detection. The PSA was recognised and detected through enzymatic cleavage of its corresponding aptamer, enabling detection of PSA in the concentration range of 10 pM to 100 nM.[72] An improved version of this system was reported by the same group by utilising a distance dependent system for the detection of the proteolytic enzyme caspase-3, closely associated with apoptotic cells (Fig. 6a). Bifunctional AuNPs were conjugated to FITC dye using ssDNA and a short peptide bond, held together <2 nm apart, resulting in quenching to enhancement. Notably, once the peptide strand had been cleaved, the nanoparticle and fluorophore were held together at a fixed distance of ~7 nm, allowing for controlled MEF. This system highlighted the advantages, primarily the small size and modifiability, of aptamers over antibodies in distance dependent systems.[73] Following this early work, in 2014, Yang *et al.* demonstrated a silver nanocluster aptamer based system for the detection of carcinoembryonic antigen (CEA).[74] Here, fluorescent silver nanoclusters used as a fluorophore, were conjugated to DNA modified gold nanoparticles by a specific aptamer, obtaining a detection limit of 3 pg mL^{-1}.

$Ag@SiO_2$ nanospheres are a widely used plasmonic structure that have attracted interest for their use in MEF biosensors over the last decade.[75] Silver produces a strong plasmonic response in the visible region and the silica coating acts as a stabiliser and spacer. By changing the thickness of the silica shell, the distance between NP and fluorophore can be controlled. In 2014, Pang *et al*. employed $Ag@SiO_2$ nanospheres in an aptasensor for the detection of recombinant hemagglutinin (rHA) protein, produced by H5N1 influenza virus.[76] Aptasensors are specifically useful in the detection of enveloped viruses, as these viruses display target proteins on their outer lipid membrane. In H5N1 influenza virus, rHA exists as trimeric spikes on the viral membrane, hence can be detected by guanine richen aptamer. In this sensor, the ability of the aptamer to undergo conformation changes under biomarker detection was exploited, resulting in the formation of a G-quadruplex complex, allowing for binding and

enhancement of thiozole orange (TO). Combining the high selectivity of rHA aptamers with high fluorescence enhancement from the core-shell $Ag@SiO_2$ nanospheres, this system showed a detection limit of 2 and 3.5 ng/mL in aqueous buffer and human serum respectively, exhibiting higher selectivity, sensitivity and a faster detection time than ELISA based H5N1 tests. The detection process could be also carried out in a tube in <30 minutes, much faster than ELISA based sensors, highlighting its effectiveness as a point-of-care diagnostic tool.[76] Similarly, in 2014, Pang *et al*. synthesised a "turn on" $Ag@SiO_2$ nanosphere sensor for the detection of Hg^{2+}.[77] Here, thiamine rich aptamers were utilised for the formation of T-Hg^{2+}-T hairpin complexes. Fluorescence enhancement of TO was observed in the visible region around 550 nm, achieving a LOD of 0.33 nM with high specificity. Later, in 2016, Sui *et al*. also demonstrated the capability of these nanostructures in an ultrasensitive thrombin aptasensor, achieving a 0.05 nM detection limit (Fig 6b).[51] In this work, thrombin aptamers and DNA-Cy5 complexes were conjugated to $Ag@SiO_2$ nanospheres, initially displaying strong metal enhanced fluorescence. Upon the addition of thrombin and graphene oxide, the DNA-Cy5 was displaced and quenched as a result of π-stacking on graphene oxide surface.[51] Although this sensor presented a high sensitivity, it required two different nanostructures, increasing complexity of the system, reducing its suitability for commercial biosensing.

Improving on the $Ag@SiO_2$ structure, in 2019, Deng *et al.* presented a multi-layer nanostructure consisting of a silver core, silica spacer and a dye doped Tris(2,2'-bipyridyl)ruthenium(II) chloride hexahydrate (RuBPy) silica outer layer, for the detection of PSA (Fig. 6c).[78] These multi-layer systems are advantageous as fluorophores can be doped in the outer silica shell, which can protect them against collisional quenching. Here, a black hole quencher (BHQ) dye, conjugated to the NP surface by an aptamer, was quenched through FRET. In the presence of PSA, this BHQ-PSA aptamer could detach and specifically bind to the PSA in solution, allowing recovery of the fluorescence signal. A detection limit of 0.2 ng ml^{-1} (6.1 pM) was attained, which was much lower than the concentration present in serum of healthy prostates (4.0 ng ml^{-1}), exhibiting the high sensitivity of this system and potential for clinical use. This system also showed a 6.7-fold increase than that of hollow RuBPy doped silica NPs by incorporating a silver core.[78] The additional doped silica layer on the outside was able to lower the detection limit by several orders of magnitude compared to those $Ag@SiO_2$ structures fabricated by Sui *et al.* [51] and Pang *et al.*[77], clearly displaying the increased sensitivity of multi-layered structures.

In recent work by Zhu *et al*., the fluorescence intensity and polarisation were both measured in a novel enzyme free assay for the detection of miRNA-21 using decahedral silver nanoparticles ($Ag_{10}NPs$) via a strand displaced reaction (Fig. 6d).[64] This sensor, comprised of two self-assembled complementary nucleic acid strands, was conjugated to the $Ag_{10}NPs$. Initially, FAM dye on the end of the second nucleic acid strand was enhanced by $Ag_{10}NPs$. Then, miRNA-21 added to the solution was able react with the 2-FAM complex, resulting in the formation of a double stranded structure free in solution, reducing fluorescence. Subsequently, miRNA-21 was released and initiated the next chain substitution reaction process. This method displayed a unique detection mechanism and achieved a detection limit of 93.8 pM in <40 minutes, highlighting the sensitivity of substitution reaction processes, whereby one target molecule can result in more than one dye enhancement reaction, amplifying the signal.[64]

PLEASE CITE THIS ARTICLE AS DOI: 10.1063/5.0065833

Clinical diagnosis of adenosine triphosphate (ATP) is extremely important as it has been reported as a biomarker for multiple diseases, including benign prostatic hyperplasia and HIV cognitive impairment.[79-80] Extracellular ATP has also been reported to significantly promote cancer progression and metastasis.[81] Traditional methods of ATP detection such as chromatography are often time consuming and complex, hence recently developed plasmonic ATP biosensors have proved simpler and more efficient alternatives. In 2014, Lu *et al*. synthesised a novel biosensor for ATP detection using a core-shell Ag@SiO_2 nanoflare via target-induced structure switching.[82] A 32-fold enhancement was achieved using Cy5 dye, however a relatively high detection limit of 8 μM with a linear response from 0 to 0.5 mM was seen.[82] Other ATP sensors using Ag@SiO_2 nanospheres have also been investigated, producing 5.8-fold enhancements and much lower detection limits of 14.2 nM.[83] More recently, in 2019, Jiang *et al*. fabricated an ATP aptasensor based on a "turn off" mechanism.[84] Here, polyA$_n$-based ATP recognition aptamers were modified onto the surface of AuNPs and conjugated with FAM-labelled aptamers, where polyA$_n$ acted as a spacer and the length was precisely controlled to maintain optimal distance between FAM and the AuNP, enabling a high initial fluorescence enhancement in the visible region. When introduced to the system, ATP molecules were able to selectively bind to the aptamer, releasing the FAM-DNA complex from the nanoparticle surface, resulting in quenching of the system. This MEF biosensor was able to achieve a detection limit of 0.2 nM and a sensitivity 7 times higher than other traditional strategies.[84]

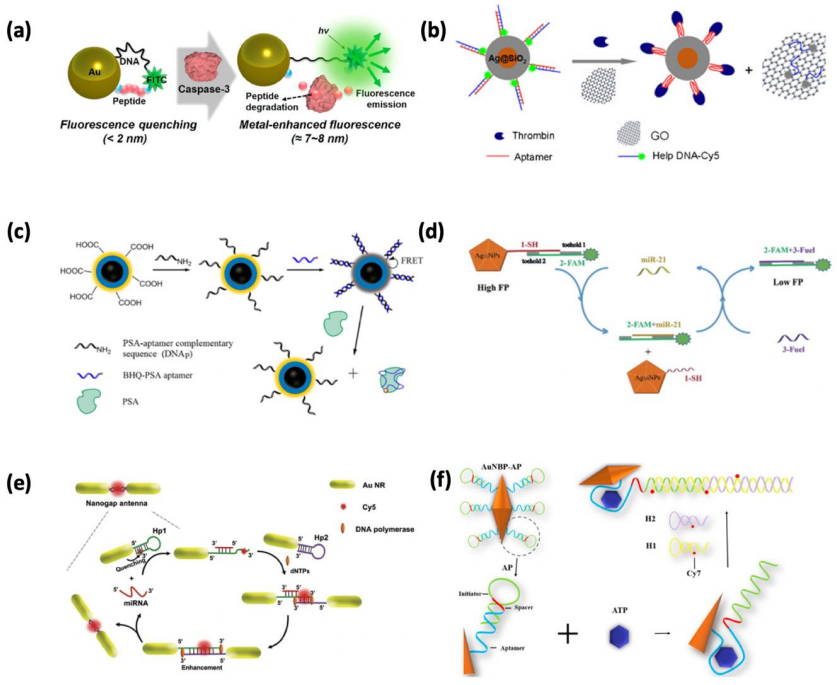

Figure 6: (a) AuNP distance dependent aptasensor for caspase-3 detection.[73] Reprinted with permission from Choi *et al.*, Nano Letters 20 (10), 7100-7107 (2020). Copyright 2020 Nano Letters. (b) Thrombin biosensor system using Ag@SiO_2 and graphene oxide for fluorescence enhancement and quenching respectively.[51] Reproduced with permission from Sui *et al.*, Microchimica Acta 183 (5), 1563-1570 (2016). Copyright 2016 Microchimica Acta. (c) Schematic of Ag@SiO_2@SiO_2-RuBpy composite nanoparticle system for the target triggered turn on detection of PSA.[78] Reproduced with permission from Deng *et al.*, Nanotechnology 28 (6), 065501 (2017). Copyright 2017 Nanotechnology. (d) Schematic of miRNA-21 sensor using strand displacement reaction. Target miRNA-21 displaces 2-FAM dye molecule resulting in reduced fluorescence.[64] Reproduced with permission from Zhu *et al.*, RSC Advances 110 (29), 17037-17044 (2020). Copyright 2020 RSC Advances. (e) Illustration of nanogap Au antenna system for the detection of miRNA.[47] Reproduced with permission from Peng *et al.*, Small 16 (19), 2000460 (2020). Copyright 2020 Small. (f) ATP biosensor using structure switching aptamers conjugated to AuNBPs.[49] Reproduced with permission from Zheng *et al.*, Sensors and Actuators B: Chemical 319, 128263 (2020). Copyright 2020 Sensors and Actuators B: Chemical.

AuNPs are frequently utilised as molecular probes for their ease of synthesis, facile surface functionalisation, precise control over size and shape as well as biocompatibility.[33] In 2016, Adegoke *et al.* reported a novel fluorescent biosensor system for DNA detection whereby L-glutathione capped AuNPs were able to conjugate to SiO_2-capped CdZnSeS/$ZnSe_{1.0}S_{1.3}$ quantum dots.[85] Quantum dots are zero-dimensional semiconductor nanocrystals a few nanometres in size, which exhibit several advantages over organic dyes such as higher quantum yields, interplay between size and luminescence, photostability and longer excited-state lifetimes. Additionally, by altering their compositions and size, the LSPR can be tuned across a wide of wavelengths.[9] In this system, the SiO_2/Quantum dot/molecular beacon probe was able to detect a DNA sequence at concentrations as low as 10 fg/mL in the visible region.[85]

Most recently, in 2021, gold nanospheres of two different sizes (20 and 60 nm) were utilised by Choi *et al.* for the development of another biosensor for the detection of breast cancer gene-1 (BRCA-1).[86] BRCA-1 is a gene that produces protein for repair of damaged DNA. Harmful mutated variants of this gene dramatically increase the probability of developing breast or ovarian cancer, thus sensitive detection of BRCA-1 and its mutations is important in facilitating early diagnosis.[87] Clustered regularly interspaced short palindromic repeats (CRISPR) of genetic information and their complexes are frequently used for gene editing due to their ability to recognise and degrade nucleic acid sequences. These properties have allowed them to be used for a wide range of biomedical applications such as cancer therapy, gene delivery and biosensing. A CRISPR-Cas12a complex was used for the first time in the separation of NP and FITC fluorophore, resulting in enhancement of the fluorescence signal and also in a visible colour change, allowing for a secondary analysis method to confirm detection. Detection as low as 0.34 fM was achieved in <30 minutes. This method is similar to previous work carried out whereby detection of the target biomarker results in the cleavage of dye labelled aptamers from AuNPs surface into solution.[86]

Previous studies have demonstrated that coupled metal nanostructures give rise to much stronger hot spots of electromagnetic field than monomeric systems, resulting in higher fluorescence enhancements. These hotspots arise due to confined electromagnetic fields

PLEASE CITE THIS ARTICLE AS DOI: 10.1063/5.0065833

between adjacent nanostructures, however these are usually found in substrate based sensors, where NPs are immobilised and can be deposited close to each other. In work carried out by Peng *et al*. in 2020, coupled gold nanorods were used in a nanogap antenna based sensor for highly sensitive microRNA detection, with detection limits as low as 97.2 x 10^{-18} M.[47] Here, hairpin DNA molecules were used to trigger a strand displacement amplification reaction, resulting in an end-to-end gold nanorod dimer with Cy5 located in the gap (Fig. 6e). This system produced a limit of detection in the attomolar range, far lower than other solution based aptasensors, highlighting the potential of these coupled systems. Another coupled nanostructure system investigated by Zhu *et al*., reported a LOD of 3.1 pM under optimum conditions.[88] The effects of nanoparticle size, shape, dye distribution and separation distance were investigated on the sensitivity of the sensor for the detection. A significant 100-fold MEF enhancement was achieved compared to quenched Cy5 using Au@Ag nanospheres and a 5-fold enhancement was achieved compared to the unquenched dye in solution.

Recently, nanobipyramids have been at the focus of attention as optical antennas for MEF due to their tunable LSPR and high intensity electromagnetic hot spots that form at their sharp corners. In 2020, Zheng *et al*. reported NIR detection of ATP for the first time by employing a structure-switching aptamer approach triggered by a hybridised chain reaction (HCR) in homogenous solution (Fig. 6f).[50] Here, gold nanobipyramids (AuNBPs) were functionalised with DNA oligonucleotide aptamers and upon ATP detection, the aptamers changed shape, initiating the chain reaction. Following this, hairpin aptamers (H1 and H2) were able to bind to the DNA aptamers bringing fluorophore Cy7 within the required distance for fluorescence enhancement to occur. A maximum fluorescence of 5.63-fold and a detection limit of 35 nM were obtained. The detection limit reported here is lower than other ATP sensors, which could be due to the complexity of the system, requiring the binding of 3 different aptamers and changes in morphology, increasing in the likelihood of false negative signals. Nonetheless, this method is easily modifiable for the detection of other biomarkers by using different aptamers and corresponding DNA strands. Furthermore, the use of a NIR dye in this system is advantageous as they produce very little background signal and allow better penetration through blood without pre-treatment.[9, 49] These solution based aptasensors exhibit high sensitivity and highly versatile detection mechanisms, however also present areas for continued development of more complex nanostructures and coupled systems, with great potential not only for highly specific disease detection but also for *in vivo* imaging.

5.2 Substrate based MEF aptasensors

Substrate based sensing offers the advantage over solution-based sensing of exhibiting areas of increased localised electromagnetic field between adjacent nanostructures, resulting in higher fluorophore enhancements and more sensitive detection. These substrates can be made highly reproducible, due to widely used lithographic techniques suitable for large scale fabrication. The ability of biosensors to multiplex and detect more than one biomarker in the same sample is crucial for accurate disease diagnosis, however the majority of aptamer sensors have been developed for single target analysis. Nonetheless, in 2016, Wang *et al*. produced an aptamer based sandwich assay for the detection of two biomarkers, thrombin and PDGF-BB, using silver nanoparticle substrates (Fig. 7a).[89] Aptamer modified silver nanoparticle substrates were used as capture probes for the target biomarkers. Upon

successful biomarker detection, secondary dye-conjugated aptamers (Cy5 and Cy3) were used as report probes. The detection limit of this sandwich assay using silver nanoparticles was found to be 80 to 8 times lower compared with aptamers directly. Detection limits of 625 pM and 21 pM were achieved for PDGF-BB and thrombin respectively.[89] Though the majority of nanostructures reported for these sensors are gold and silver based, cost effective alternatives with similar plasmonic properties are desirable for commercial viability. In 2019, an aluminium multiplexed biosensor was produced by Siddique *et al.* for the detection of insulin, vascular endothelial growth factor and thrombin (Fig. 7b). Here, DNA aptamers tagged with FAM, Cy3 and Cy5 were conjugated to the aluminium nanoantennae substrates. This sensor presented a 1000-fold broadband enhancement in the visible range and a detection limit of 100 pM, showing great potential for highly sensitive, multiplexed, on-chip clinical diagnostics.[90]

Gold nanotriangle (AuNT) arrays in particular have been widely investigated as plasmonic substrates for biosensing due to the high intensity electromagnetic hot spots that arise at their corners.[48, 91] In 2020, Masterson *et al.* demonstrated their capability in a gold triangular nanoprism based sensor, for the detection of oncogenic microRNAs at sub-fg μL $^{-1}$ concentrations from patient plasma. Here, ssDNA was used to selectively bind the microRNA target molecules to the substrate and target detection was established through surface-enhanced Raman scattering (SERS) and MEF.[92] However, this substrate exhibits a low reproducibility due to the random arrangement of nanoparticles and could be improved by using lithographic fabrication methods, such as those utilised by Xie *et al.*[48]

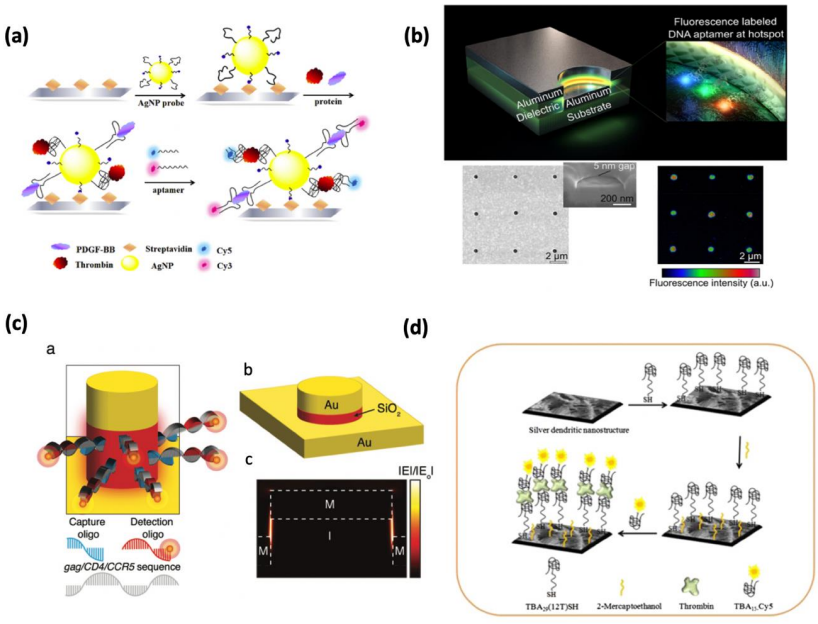

Figure 7: (a) Schematic of multiplexed sandwich aptamer system for the detection of thrombin and PDGF-BB.[89] Reproduced with permission from Wang *et al.*, Analytica Chimica Acta 905, 149-155 (2016). Copyright 2016 Analytica Chimica Acta. (b) Schematic of aluminium nanodiscs separated by dielectric layer allowing for electromagnetic hotspots and biomolecule capture.[90] Reprinted with permission from Siddique *et al.*, from ACS Nano 13 (12), 13775-13783 (2019). Copyright 2019 ACS Nano. (c) Au-SiO_2-Au nanodisc biosensor for the detection of nucleic acids a) Schematic of nucleic acid sequence conjugation to nanostructure b) Nanostructure configuration consisting of Au nanodisc coupled with Au nanohole separated by a dielectric SiO_2 nanogap c) The electric field intensity is displayed.[46] Reproduced with permission from Narasimhan *et al.*, Nanoscale 11 (29), 13750-13757 (2019). Copyright 2019 Nanoscale. (d) Illustration of thrombin biosensor based on silver dendritic nanostructures.[50] Reproduced with permission from Lofti *et al.*, Plasmonics 14 (3), 561-568 (2019). Copyright 2019 Plasmonics.

Gold nanodiscs (AuNDs) were utilised by Narasimhan *et al*. in 2019 for broadband detection of nucleic acid analytes using quadrupolar modal gap-plasmons on biomimetic gold metasurfaces (Fig. 7c). Broad band detection is highly desirable for biosensing as it can be used to enhance multiple fluorophores over a broad wavelength range, enabling multiplexing. Here, a broad band plasmonic peak from 550 - 850 nm allowed for three different HIV-1 biomarkers to be detected on a single chip. To selectively immobilise and detect the target nucleic acids, DNA/RNA hybridisation reactions were used in a sandwich assay format. The detection of biomarkers was demonstrated at concentrations as low as 10 pM.[46] Other gold based aptasensor platforms have been investigated, combining graphene oxide as an interfacial quencher, allowing active tuning of the quenching-to-enhancing region achieving amplified signal-to-noise ratios of >1000 fold.[93]

Recently, in 2020, Minopoli *et al*. presented a gold based aptasensor to detect malaria biomarker plasmodium falciparum lactate dehydrogenase (*Pf*LDH), using a combination of antibodies and aptamers.[94] The combination of aptamers and antibodies has demonstrated to be a useful approach in molecular recognition due to their high sensitivity and selectivity, however these aptamer-antibody sensors have not been documented for MEF based sensors. Malaria is still one of the main causes of disease-related deaths worldwide and there is an urgent need for sensors to be able to detect *Pf*LDH at picomolar levels in patient serum. In this work, AuNP substrates were synthesised using block co-polymer micelle lithography, a cost-effective, scalable and tunable method for producing plasmonic substrates. A limit of detection of <30 fM was reported, several orders of magnitude lower than rapid malaria diagnostic tests and commercial ELISA kits. This device could also be used in automated well-plate readers, improving its ease of use for clinical purposes.[94]

Moving away from gold substrates, Lofti *et al*. reported a silver dendritic nanosensor for thrombin detection (Fig. 7d).[50] Here, thiolated 29-mer aptamers were used as biorecognition molecules and conjugated to the silver nanostructures. Upon detection, thrombin was then sandwiched between the capture aptamer and a Cy5-labelled thrombin aptamer, reporting a detection limit of 32 pM. Though this platform displays high sensitivity, low-cost and ease of fabrication, the random formation of silver dendrites results in low reproducibility, limiting its applicability as a tool for clinical diagnosis.[50] A similar nanostructure was fabricated by Ji *et al.* for improved protein and DNA detection. Here, silver nanorods were deposited on

PLEASE CITE THIS ARTICLE AS DOI: 10.1063/5.0065833

substrates at an angle, achieving a 14-fold fluorophore enhancement and a detection limit of 0.01 pM via the hybridisation of single-stranded oligonucleotides.[95] Most recently, in 2020, Harpaz *et al*. produced a novel silver complementary-metal-oxide-based-semiconductor (CMOS) biosensor, integrating specific DNA strands for the detection of enoyl-CoA-isomerase.[96] While CMOS devices are usually used in electronics, their ease of manufacture and scalability make them ideal for commercial biosensor substrates. Here, DNA strands were immobilised onto silver CMOS substrates, allowing reporter DNA conjugated with horseradish peroxidase (HRP) enzyme to bind, bringing the enzyme in close proximity to nanoparticle substrate. Light signal produced from the enzyme could be both amplified and detected by the silver CMOS substrate, achieving a detection limit of 3.3 nM.[96] This work and other substrate based aptasensors reviewed here have presented lower detection limits and higher reproducibility than most of the solution based sensors reviewed. Additionally, the incorporation multiplexed sensing highlights their capability for sensitive and accurate clinical diagnoses.

Table II: Comparison of substrate and solution based MEF aptasensors and their features, as described in this review.

Plasmonic structure	Nanoparticle diameter size	Target biomarker	Sensor platform	Fluorophore	Detection mechanism	LOD	Detection time	Ref.
AuNP	48 nm	*Pf*LDH	Solution	Cy5	Sandwich assay	30 fM	< 3 h	[94]
"	60 nm	PSA	"	FITC	'Turn on'	10 pM – 100 nM	-	[72]
"	30 nm	Caspase-3	"	FITC	'Turn on'	10 pg/mL	-	[73]
"	20 nm, 60 nm	BRCA-1	"	FITC	CRISPR-Cas12a complex	0.34 fM	30 min	[86]
"	11 -15 nm	CEA	"	Ag nanoclusters	'Turn on'	3 pg mL^{-1}	-	[74]
"	20 nm	ATP	"	FAM	'Turn off'	0.2 nM	-	[84]
"	9.2 nm	DNA	"	$CdZnSeS/ZnSe_{1.0}S_{1.3}$	DNA hybridisation	1.4 fM	-	[85]
AuNR	27 x 12 nm	microRNA	"	Cy5	Strand displacement reaction	0.0972 fM	-	[47]
Au@Ag	65 nm	DNA	"	Cy5	'Turn on'	3.1 pM	-	[88]
$Ag_{10}NPs$	55.3 ± 4.0 nm	miRNA-21	"	FAM	Strand displacement reaction	93.8 pM	40 min	[64]
$Ag@SiO_2$	49 ± 8 nm	Thrombin	"	Cy5	'Turn off'	0.05 nM	-	[51]
"	75 – 155 nm	rHA	"	TO	'Turn on'	2 – 3.5 ng/mL	30 min	[76]
"	66 nm	ATP	"	Cy5	-	8 µM	-	[82]
"	54 – 82 nm	ATP	"	PicoGreen	'Turn off'	14.2 nM	-	[83]
"	30 ± 2 nm	Hg^{2+}	"	TO	'Turn on'	0.33 nM	30 min	[77]
AuNBP	~100 x 50 nm	ATP	"	Cy7	HCR	35 nM	26 h	[49]
RuBPy	62 – 100 nm	PSA	"	BHQ	'Turn on'	6.1 pM	-	[78]
AuNT	8, 42 nm	microRNA	Substrate	FAM	'Turn on'	sub-fg μL^{-1}	-	[92]
Au nanodiscs	50 – 400 nm	DNA	"	AF 555, 750, 790	HCR	10 pM – 10 µM	-	[46]
Au film	-	DNA	"	-	'Turn on'	10 pM	-	[93]
Ag dendrites	105 nm	Thrombin	"	Cy5	'Turn on'	32 pM	-	[50]
Ag zigzags	-	DNA	"	AF 488	DNA hybridisation	0.01 pM	-	[95]
AgNP	20 nm	Thrombin, PDGF	"	Cy3, Cy5	'Turn on'	625 pM, 21 pM	-	[89]
Al film	3 nm	Insulin, VEGF, thrombin	"	FAM, Cy3, Cy5	'Turn on'	100 pM	-	[90]
Ag CMOS	-	Enoyl-CoA-isomerase	"	HRP	'Turn on'	3.3 nM	-	[96]

PLEASE CITE THIS ARTICLE AS DOI: 10.1063/5.0065833

5. Challenges and future outlook

Aptamer biosensing based on MEF platforms have revolutionised the field of early detection. Aptamers offer several advantages over other biorecognition molecules, primarily their high specificity and detection times, owing to their ability to undergo diverse and complex conformational changes upon target recognition. In addition, mechanisms such as target induced structure switching reactions have shown great potential to amplify fluorophore signals. When combined with MEF, aptamers allow for quenching to signal enhancement mechanisms, whereby the system background noise can be reduced to zero, vastly increasing sensitivity.

Nevertheless, in order to upscale their production for clinical settings, their limitations should also be considered. One of the biggest barriers for the use of aptamers in biosensing is that aptamer databases are limited and there are several biomarkers for which there are no corresponding aptamers. For example, there are currently no aptamers that have been prospectively validated in biological fluids for the detection of pancreatic cancer biomarker CA 19-9. For continued large-scale use of aptasensors for a variety of diseases, an extensive database of aptamers and their corresponding biomarkers is needed. Increased use of automated SELEX and capillary electrophoresis SELEX has potential to improve the specificity of these aptamers and shorten the selection process. Furthermore, it is crucial to develop synthesis and purification methods to enable uniformity across nanostructures for solution and substrate-based sensors. These sensors should be robust, reproducible and able to be upscaled cheaply for commercialisation, without compromising on their plasmonic properties. Though large arrays of NPs can be produced on a substrate using top-down lithographic techniques, these can be expensive. Through development of low-cost deposition methods, regular NP arrays can be produced allowing for repeatable readings across the substrate and enabling sensitive calibration of fluorescence intensity with biomarker concentrations.

Despite vast progress made in the synthesis of NPs structures, there are few MEF aptasensors that are capable of multiplexed detection. This gap in research highlights the need to develop broadband plasmonic structures for detection of more than one fluorophore for even more reliable diagnosis. Coupled structures in particular have shown to produce very low detection limits, hence will undoubtedly be an area of interest in the future particularly in solution-based sensing where NPs are further apart. MEF aptasensors have shown great potential for highly specific and sensitive sensing and by overcoming the engineering and real-world clinical challenges addressed here, it will open up the possibility for earlier diagnosis, treatment and monitoring of diseases, with the potential to save countless lives.

References

1. Kazarian, A.; Blyuss, O.; Metodieva, G.; Gentry-Maharaj, A.; Ryan, A.; Kiseleva, E. M.; Prytomanova, O. M.; Jacobs, I. J.; Widschwendter, M.; Menon, U.; Timms, J. F., *British Journal of Cancer* **2017,** *116* (4), 501-508.
2. Pereira, S. P.; Oldfield, L.; Ney, A.; Hart, P. A.; Keane, M. G.; Pandol, S. J.; Li, D.; Greenhalf, W.; Jeon, C. Y.; Koay, E. J.; Almario, C. V.; Halloran, C.; Lennon, A. M.; Costello, E., *The Lancet Gastroenterology & Hepatology* **2020,** *5* (7), 698-710.
3. Capriglione, S.; Luvero, D.; Plotti, F.; Terranova, C.; Montera, R.; Scaletta, G.; Schirò, T.; Rossini, G.; Benedetti Panici, P.; Angioli, R., *Medical Oncology* **2017,** *34* (9), 164.
4. Sammon Jesse, D.; Serrell Emily, C.; Karabon, P.; Leow Jeffrey, J.; Abdollah, F.; Weissman Joel, S.; Han Paul, K. J.; Hansen, M.; Menon, M.; Trinh, Q.-D., *Journal of Urology* **2018,** *199* (1), 81-88.
5. Qian, L.; Li, Q.; Baryeh, K.; Qiu, W.; Li, K.; Zhang, J.; Yu, Q.; Xu, D.; Liu, W.; Brand, R. E.; Zhang, X.; Chen, W.; Liu, G., *Translational Research* **2019,** *213*, 67-89.
6. Damborský, P.; Švitel, J.; Katrlík, J., *Essays Biochem* **2016,** *60* (1), 91-100.
7. Mehrotra, P., *J Oral Biol Craniofac Res* **2016,** *6* (2), 153-159.
8. Aydin, S., *Peptides* **2015,** *72*, 4-15.
9. Fothergill, S. M.; Joyce, C.; Xie, F., *Nanoscale* **2018,** *10* (45), 20914-20929.
10. Bauch, M.; Toma, K.; Toma, M.; Zhang, Q.; Dostalek, J., *Plasmonics* **2014,** *9* (4), 781-799.
11. Keefe, A. D.; Pai, S.; Ellington, A., *Nature Reviews Drug Discovery* **2010,** *9* (7), 537-550.
12. Zhao, X.; Dai, X.; Zhao, S.; Cui, X.; Gong, T.; Song, Z.; Meng, H.; Zhang, X.; Yu, B., *Spectrochimica Acta Part A: Molecular and Biomolecular Spectroscopy* **2021,** *247*, 119038.
13. Tuerk, C.; Gold, L., *Science* **1990,** *249* (4968), 505.
14. Song, K.-M.; Lee, S.; Ban, C., *Sensors (Basel)* **2012,** *12* (1), 612-631.
15. Song, S.; Wang, L.; Li, J.; Fan, C.; Zhao, J., *TrAC Trends in Analytical Chemistry* **2008,** *27* (2), 108-117.
16. Ko Ferrigno, P., *Essays Biochem* **2016,** *60* (1), 19-25.
17. Jovčevska, I.; Muyldermans, S., *BioDrugs* **2020,** *34* (1), 11-26.
18. Nguyen, H. H.; Lee, S. H.; Lee, U. J.; Fermin, C. D.; Kim, M., *Materials (Basel)* **2019,** *12* (1), 121.
19. Ispas, C. R.; Crivat, G.; Andreescu, S., *Analytical Letters* **2012,** *45* (2-3), 168-186.
20. Reyes-De-Corcuera, J. I.; Olstad, H. E.; García-Torres, R., *Annual Review of Food Science and Technology* **2018,** *9* (1), 293-322.
21. Chandrasekaran, A. R.; Anderson, N.; Kizer, M.; Halvorsen, K.; Wang, X., *ChemBioChem* **2016,** *17* (12), 1081-1089.
22. Thacker, V. V.; Herrmann, L. O.; Sigle, D. O.; Zhang, T.; Liedl, T.; Baumberg, J. J.; Keyser, U. F., *Nature Communications* **2014,** *5* (1), 3448.
23. Loretan, M.; Domljanovic, I.; Lakatos, M.; Rüegg, C.; Acuna, G. P., *Materials* **2020,** *13* (9).
24. Ramakrishnan, S.; Ijäs, H.; Linko, V.; Keller, A., *Comput Struct Biotechnol J* **2018,** *16*, 342-349.
25. Wang, D.; Da, Z.; Zhang, B.; Isbell, M. A.; Dong, Y.; Zhou, X.; Liu, H.; Heng, J. Y. Y.; Yang, Z., *RSC Advances* **2015,** *5* (72), 58734-58737.

26. Arshavsky-Graham, S.; Urmann, K.; Salama, R.; Massad-Ivanir, N.; Walter, J.-G.; Scheper, T.; Segal, E., *Analyst* **2020,** *145* (14), 4991-5003.
27. Chhasatia, R.; Sweetman, M. J.; Harding, F. J.; Waibel, M.; Kay, T.; Thomas, H.; Loudovaris, T.; Voelcker, N. H., *Biosens Bioelectron* **2017,** *91*, 515-522.
28. Dhar, P.; Samarasinghe, R. M.; Shigdar, S., *International Journal of Molecular Sciences* **2020,** *21* (7).
29. Molefe, P. F.; Masamba, P.; Oyinloye, B. E.; Mbatha, L. S.; Meyer, M.; Kappo, A. P., *Pharmaceuticals (Basel)* **2018,** *11* (4), 93.
30. Lakhin, A. V.; Tarantul, V. Z.; Gening, L. V., *Acta Naturae* **2013,** *5* (4), 34-43.
31. Geddes, C. D., *Physical Chemistry Chemical Physics* **2013,** *15* (45), 19537-19537.
32. Geddes, C. D.; Lakowicz, J. R., *Journal of Fluorescence* **2002,** *12* (2), 121-129.
33. Joyce, C.; Fothergill, S. M.; Xie, F., *Materials Today Advances* **2020,** *7*, 100073.
34. Shen, H.; Guillot, N.; Rouxel, J.; Lamy de la Chapelle, M.; Toury, T., *Opt. Express* **2012,** *20* (19), 21278-21290.
35. Jawad, Z. A. R.; Theodorou, I. G.; Jiao, L. R.; Xie, F., *Scientific Reports* **2017,** *7* (1), 14309.
36. Brien, D. P.; Sandanayake, N. S.; Jenkinson, C.; Gentry-Maharaj, A.; Apostolidou, S.; Fourkala, E.-O.; Camuzeaux, S.; Blyuss, O.; Gunu, R.; Dawnay, A.; Zaikin, A.; Smith, R. C.; Jacobs, I. J.; Menon, U.; Costello, E.; Pereira, S. P.; Timms, J. F., *Clinical Cancer Research* **2015,** *21* (3), 622.
37. Yaraki, M. T.; Tan, Y. N., *Chemistry – An Asian Journal* **2020,** *15* (20), 3180-3208.
38. Della Ventura, B.; Gelzo, M.; Battista, E.; Alabastri, A.; Schirato, A.; Castaldo, G.; Corso, G.; Gentile, F.; Velotta, R., *ACS Applied Materials & Interfaces* **2019,** *11* (4), 3753-3762.
39. Yun, B. J.; Kwon, J. E.; Lee, K.; Koh, W.-G., *Sensors and Actuators B: Chemical* **2019,** *284*, 140-147.
40. Xie, F.; Baker, M. S.; Goldys, E. M., *Chemistry of Materials* **2008,** *20* (5), 1788-1797.
41. De Marchi, S.; Núñez-Sánchez, S.; Bodelón, G.; Pérez-Juste, J.; Pastoriza-Santos, I., *Nanoscale* **2020,** *12* (46), 23424-23443.
42. Sugawa, K.; Tamura, T.; Tahara, H.; Yamaguchi, D.; Akiyama, T.; Otsuki, J.; Kusaka, Y.; Fukuda, N.; Ushijima, H., *ACS Nano* **2013,** *7* (11), 9997-10010.
43. Sugawa, K.; Matsubara, M.; Tahara, H.; Kanai, D.; Honda, J.; Yokoyama, J.; Kanakubo, K.; Ozawa, H.; Watanuki, Y.; Kojima, Y.; Nishimiya, N.; Sagara, T.; Takase, K.; Haga, M.-a.; Otsuki, J., *ACS Applied Energy Materials* **2019,** *2* (9), 6472-6483.
44. Xu, C.; Qiu, G.; Ng, S. P.; Lawrence Wu, C.-M., *Ceramics International* **2020,** *46* (13), 20993-20999.
45. Liu, Y.; Liu, M.; Swihart, M. T., *The Journal of Physical Chemistry C* **2017,** *121* (25), 13435-13447.
46. Narasimhan, V.; Siddique, R. H.; Hoffmann, M.; Kumar, S.; Choo, H., *Nanoscale* **2019,** *11* (29), 13750-13757.
47. Peng, M.; Sun, F.; Na, N.; Ouyang, J., *Small* **2020,** *16* (19), 2000460.
48. Xie, F.; Pang, J. S.; Centeno, A.; Ryan, M. P.; Riley, D. J.; Alford, N. M., *Nano Research* **2013,** *6* (7), 496-510.
49. Zheng, M.; Kang, Y.; Liu, D.; Li, C.; Zheng, B.; Tang, H., *Sensors and Actuators B: Chemical* **2020,** *319*, 128263.
50. Lotfi, A.; Nikkhah, M.; Moshaii, A., *Plasmonics* **2019,** *14* (3), 561-568.

51. Sui, N.; Wang, L.; Xie, F.; Liu, F.; Xiao, H.; Liu, M.; Yu, W. W., *Microchimica Acta* **2016,** *183* (5), 1563-1570.
52. Chow, T. H.; Li, N.; Bai, X.; Zhuo, X.; Shao, L.; Wang, J., *Accounts of Chemical Research* **2019,** *52* (8), 2136-2146.
53. Zhu, X.; Yip, H. K.; Zhuo, X.; Jiang, R.; Chen, J.; Zhu, X.-M.; Yang, Z.; Wang, J., *Journal of the American Chemical Society* **2017,** *139* (39), 13837-13846.
54. Zheng, P.; Tang, H.; Liu, B.; Kasani, S.; Huang, L.; Wu, N., *Nano Research* **2019,** *12* (1), 63-68.
55. Nguyen, M.-K.; Su, W.-N.; Chen, C.-H.; Rick, J.; Hwang, B.-J., *Spectrochimica Acta Part A: Molecular and Biomolecular Spectroscopy* **2017,** *175*, 239-245.
56. Xu, Y.-K.; Hwang, S.; Kim, S.; Chen, J.-Y., *ACS Applied Materials & Interfaces* **2014,** *6* (8), 5619-5628.
57. Li, H.; Chen, Q.; Hassan, M. M.; Ouyang, Q.; Jiao, T.; Xu, Y.; Chen, M., *Analytica Chimica Acta* **2018,** *1018*, 94-103.
58. Genç, A.; Patarroyo, J.; Sancho-Parramon, J.; Bastús, N. G.; Puntes, V.; Arbiol, J., *Nanophotonics* **2017,** *6* (1), 193-213.
59. Pang, J. S.; Theodorou, I. G.; Centeno, A.; Petrov, P. K.; Alford, N. M.; Ryan, M. P.; Xie, F., *ACS Applied Materials & Interfaces* **2019,** *11* (26), 23083-23092.
60. Shi, J.; Tian, F.; Lyu, J.; Yang, M., *Journal of Materials Chemistry B* **2015,** *3* (35), 6989-7005.
61. Zhou, W.; Jimmy Huang, P.-J.; Ding, J.; Liu, J., *Analyst* **2014,** *139* (11), 2627-2640.
62. Roxo, C.; Kotkowiak, W.; Pasternak, A., *Molecules* **2019,** *24* (20), 3781.
63. Evanko, D., *Nature Methods* **2004,** *1* (3), 186-186.
64. Zhu, Q.; Li, H.; Xu, D., *RSC Advances* **2020,** *10* (29), 17037-17044.
65. Jeong, Y.; Kook, Y.-M.; Lee, K.; Koh, W.-G., *Biosensors and Bioelectronics* **2018,** *111*, 102-116.
66. Wang, W.; Wang, Y.; Pan, H.; Cheddah, S.; Yan, C., *Microchimica Acta* **2019,** *186* (8), 544.
67. Yang, L.; Li, N.; Wang, K.; Hai, X.; Liu, J.; Dang, F., *Talanta* **2018,** *179*, 531-537.
68. Danesh, N. M.; Yazdian-Robati, R.; Ramezani, M.; Alibolandi, M.; Abnous, K.; Taghdisi, S. M., *Sensors and Actuators B: Chemical* **2018,** *256*, 408-412.
69. Jin, H.; Gui, R.; Gong, J.; Huang, W., *Biosensors and Bioelectronics* **2017,** *92*, 378-384.
70. Yang, D.; Liu, M.; Xu, J.; Yang, C.; Wang, X.; Lou, Y.; He, N.; Wang, Z., *Talanta* **2018,** *185*, 113-117.
71. Wang, Y.; Li, Z.; Li, H.; Vuki, M.; Xu, D.; Chen, H.-Y., *Biosensors and Bioelectronics* **2012,** *32* (1), 76-81.
72. Choi, J. H.; Kim, H. S.; Choi, J.-W.; Hong, J. W.; Kim, Y.-K.; Oh, B.-K., *Biosensors and Bioelectronics* **2013,** *49*, 415-419.
73. Choi, J.-H.; Choi, J.-W., *Nano Letters* **2020,** *20* (10), 7100-7107.
74. Yang, X.; Zhuo, Y.; Zhu, S.; Luo, Y.; Feng, Y.; Xu, Y., *Biosensors and Bioelectronics* **2015,** *64*, 345-351.
75. Aslan, K.; Wu, M.; Lakowicz, J. R.; Geddes, C. D., *Journal of the American Chemical Society* **2007,** *129* (6), 1524-1525.
76. Pang, Y.; Rong, Z.; Wang, J.; Xiao, R.; Wang, S., *Biosensors and Bioelectronics* **2015,** *66*, 527-532.
77. Pang, Y.; Rong, Z.; Xiao, R.; Wang, S., *Scientific Reports* **2015,** *5* (1), 9451.

78. Deng, Y.-L.; Xu, D.-D.; Pang, D.-W.; Tang, H.-W., *Nanotechnology* **2017,** *28* (6), 065501.
79. Velasquez, S.; Prevedel, L.; Valdebenito, S.; Gorska, A. M.; Golovko, M.; Khan, N.; Geiger, J.; Eugenin, E. A., *EBioMedicine* **2020,** *51*.
80. Sugaya, K.; Nishijima, S.; Kadekawa, K.; Miyazato, M.; Mukouyama, H., *Biomedical Research* **2009,** *30* (5), 287-294.
81. Qian, Y.; Wang, X.; Li, Y.; Cao, Y.; Chen, X., *Molecular Cancer Research* **2016,** *14* (11), 1087.
82. Lu, L.; Qian, Y.; Wang, L.; Ma, K.; Zhang, Y., *ACS Applied Materials & Interfaces* **2014,** *6* (3), 1944-1950.
83. Song, Q.; Peng, M.; Wang, L.; He, D.; Ouyang, J., *Biosensors and Bioelectronics* **2016,** *77*, 237-241.
84. Jiang, L.; Hang, X.; Zhang, P.; Zhang, J.; Wang, Y.; Wang, W.; Ren, L., *Microchemical Journal* **2019,** *148*, 285-290.
85. Adegoke, O.; Park, E. Y., *Nanoscale Research Letters* **2016,** *11* (1), 523.
86. Choi, J.-H.; Lim, J.; Shin, M.; Paek, S.-H.; Choi, J.-W., *Nano Letters* **2021,** *21* (1), 693-699.
87. Kuchenbaecker, K. B.; Hopper, J. L.; Barnes, D. R.; Phillips, K. A.; Mooij, T. M.; Roos-Blom, M. J.; Jervis, S.; van Leeuwen, F. E.; Milne, R. L.; Andrieu, N.; Goldgar, D. E.; Terry, M. B.; Rookus, M. A.; Easton, D. F.; Antoniou, A. C.; McGuffog, L.; Evans, D. G.; Barrowdale, D.; Frost, D.; Adlard, J.; Ong, K. R.; Izatt, L.; Tischkowitz, M.; Eeles, R.; Davidson, R.; Hodgson, S.; Ellis, S.; Nogues, C.; Lasset, C.; Stoppa-Lyonnet, D.; Fricker, J. P.; Faivre, L.; Berthet, P.; Hooning, M. J.; van der Kolk, L. E.; Kets, C. M.; Adank, M. A.; John, E. M.; Chung, W. K.; Andrulis, I. L.; Southey, M.; Daly, M. B.; Buys, S. S.; Osorio, A.; Engel, C.; Kast, K.; Schmutzler, R. K.; Caldes, T.; Jakubowska, A.; Simard, J.; Friedlander, M. L.; McLachlan, S. A.; Machackova, E.; Foretova, L.; Tan, Y. Y.; Singer, C. F.; Olah, E.; Gerdes, A. M.; Arver, B.; Olsson, H., *Jama* **2017,** *317* (23), 2402-2416.
88. Zhu, Z.; Yuan, P.; Li, S.; Garai, M.; Hong, M.; Xu, Q.-H., *ACS Applied Bio Materials* **2018,** *1* (1), 118-124.
89. Wang, Y.; Li, H.; Xu, D., *Analytica Chimica Acta* **2016,** *905*, 149-155.
90. Siddique, R. H.; Kumar, S.; Narasimhan, V.; Kwon, H.; Choo, H., *ACS Nano* **2019,** *13* (12), 13775-13783.
91. Theodorou, I. G.; Jawad, Z. A. R.; Qin, H.; Aboagye, E. O.; Porter, A. E.; Ryan, M. P.; Xie, F., *Nanoscale* **2016,** *8* (26), 12869-12873.
92. Masterson, A. N.; Liyanage, T.; Berman, C.; Kaimakliotis, H.; Johnson, M.; Sardar, R., *Analyst* **2020,** *145* (12), 4173-4180.
93. Cao, S.-H.; Weng, Y.-H.; Xie, K.-X.; Wang, Z.-C.; Pan, X.-H.; Chen, M.; Zhai, Y.-Y.; Xu, L.-T.; Li, Y.-Q., *ACS Applied Bio Materials* **2019,** *2* (2), 625-629.
94. Minopoli, A.; Della Ventura, B.; Lenyk, B.; Gentile, F.; Tanner, J. A.; Offenhäusser, A.; Mayer, D.; Velotta, R., *Nature Communications* **2020,** *11* (1), 6134.
95. Ji, X.; Xiao, C.; Lau, W.-F.; Li, J.; Fu, J., *Biosensors and Bioelectronics* **2016,** *82*, 240-247.
96. Harpaz, D.; Alkan, N.; Eltzov, E., *Biosensors* **2020,** *10* (12).

PLEASE CITE THIS ARTICLE AS DOI: 10.1063/5.0065833

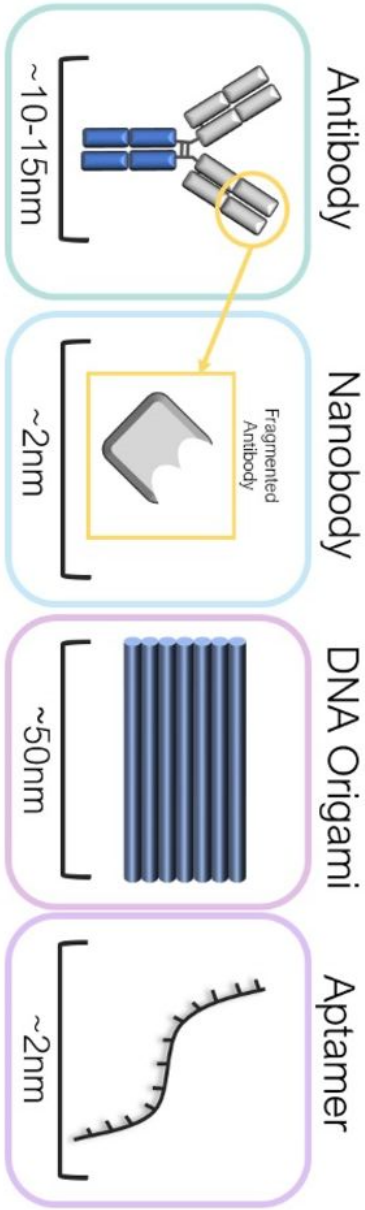

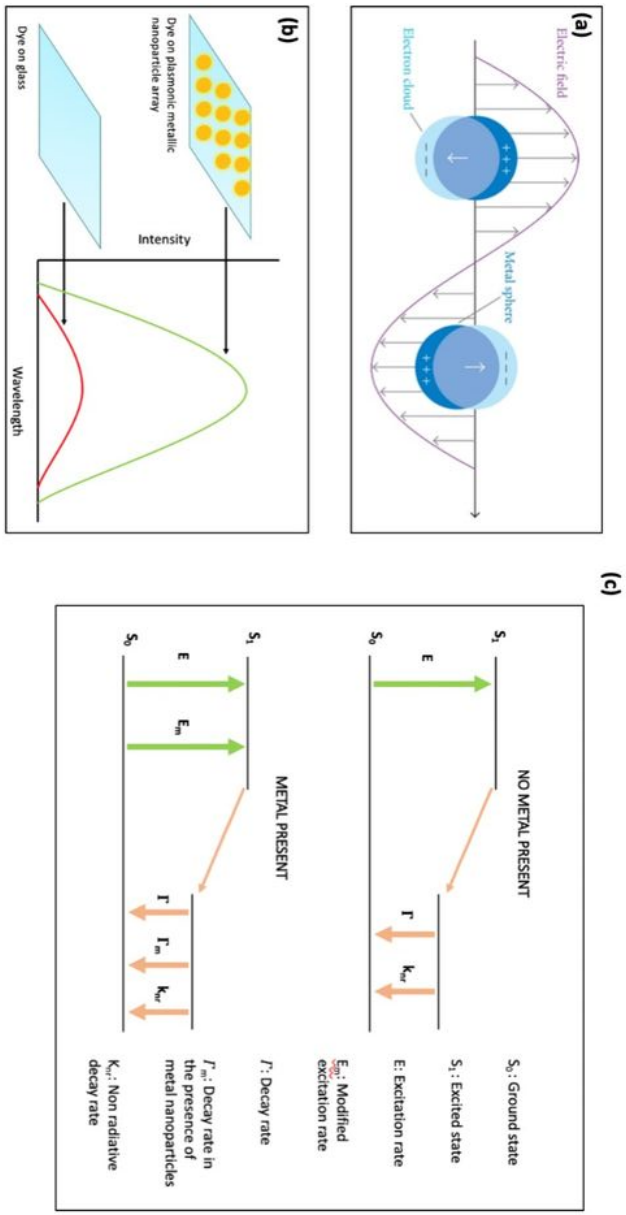

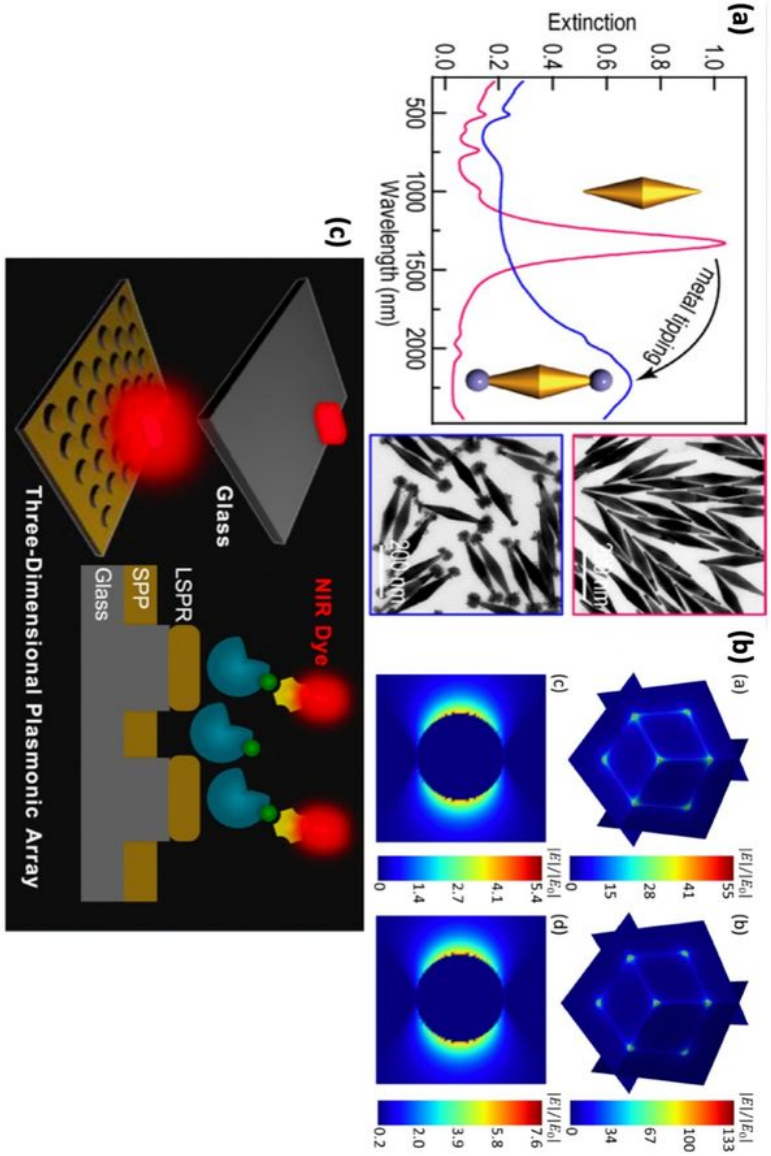

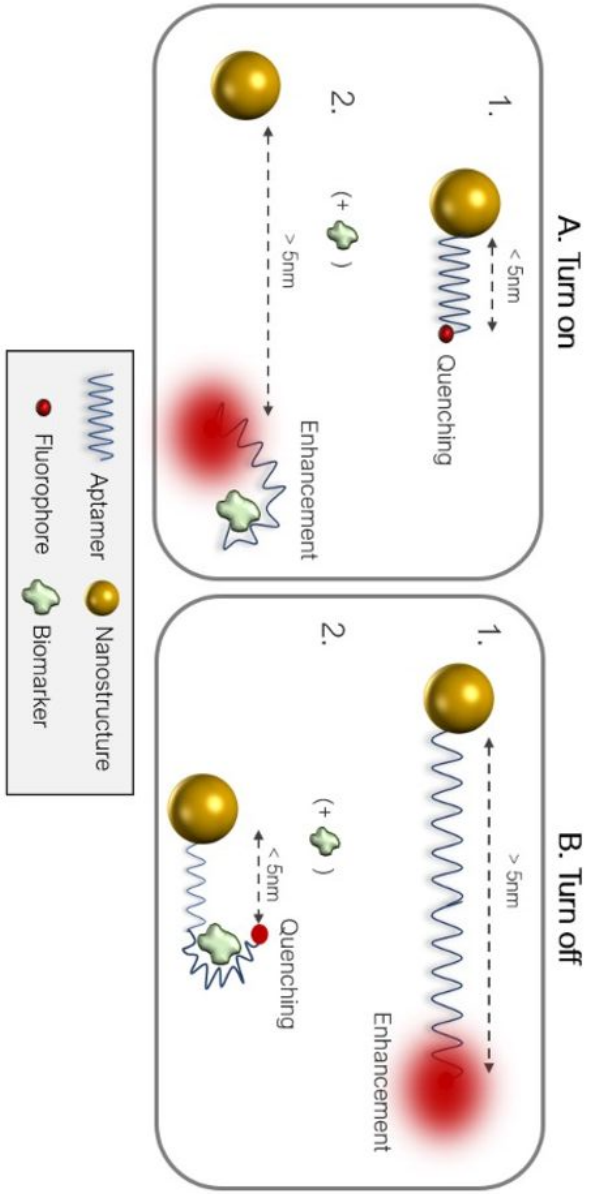

PLEASE CITE THIS ARTICLE AS DOI: 10.1063/5.0065833